Singular value decomposition of single view polarized fluorescence microscopes

Talon Chandler, Min Guo, Hari Shroff, Rudolf Oldenbourg, Patrick La Rivière

May 28, 2018

1 Introduction

In these notes we will develop the continuous models for single view polarized fluorescence microscopes with either polarized illumination or polarized detection. We will start by writing an integral transform that maps object space to data space. Then we will calculate the kernels of the integral transform and their corresponding transfer functions. Finally we will calculate the singular value decomposition of the forward operator to find the limits of these designs.

We will make use of the real circular harmonic functions

$$z_n(\theta) = \begin{cases} \frac{1}{\sqrt{\pi}}\cos(n\theta), & n > 0, \\ \frac{1}{\sqrt{2\pi}}, & n = 0, \\ \frac{1}{\sqrt{\pi}}\sin(n\theta), & n < 0. \end{cases} \tag{1}$$

The real circular harmonic functions form an orthonormal basis for functions on the circle because

$$\int_{\mathbb{S}^1} d\hat{\mathbf{p}}\, z_n(\hat{\mathbf{p}}) z_{n'}(\hat{\mathbf{p}}) = \delta_{nn'}. \tag{2}$$

Notice that we allow $z_n(\cdot)$ to take a vector argument similar to the spherical harmonics $y_l^m(\hat{\mathbf{s}}_o)$. This allows us to use these functions without specifying a coordinate system. Also notice that we are using n to index the circular harmonic functions—in a previous note set we used n to index frames or views.

2 General forward model

We will consider the problem of imaging a two-dimensional field of oriented fluorophores. To a good approximation these objects can be represented by a member of the set $\mathbb{U} = \mathbb{L}_2(\mathbb{R}^2 \times \mathbb{S}^2)$—square-integrable functions that assign a scalar value to each position and orientation.

These microscopes can collect a two-dimensional frame of intensity measurements for each position of a single polarizer on the illumination or detection arm. Therefore, the collected data is a member of the set $\mathbb{V} = \mathbb{L}_2(\mathbb{R}^2 \times \mathbb{S}^1)$—square-integrable functions that assign a scalar value to each two-dimensional position on a circle. Notice that we are considering the largest possible data space for these microscopes—a continuous sampling of the spatial and polarizer dimensions. This approach allows us to answer questions about the limits of these microscopes without considering specific choices of spatial sampling (pixels) or polarization sampling (polarizer settings). It will be helpful to think of the space $\mathbb{L}_2(\mathbb{R}^2 \times \mathbb{S}^1)$ geometrically as a continuous list of images arranged face to face in a donut—if we slice the donut along the smaller dimension (not like a pre-cut bagel!) we can see a single image taken with a single polarizer setting.

If the imaging system is spatially shift-invariant, then the forward and adjoint operators are given by the following integral transforms

$$g(\mathbf{r}_d, \hat{\mathbf{p}}) = [\mathcal{H}f](\mathbf{r}_d, \hat{\mathbf{p}}) = \int_{\mathbb{S}^2} d\hat{\mathbf{s}}_o \int_{\mathbb{R}^2} d\mathbf{r}_o\, h(\mathbf{r}_d - \mathbf{r}_o, \hat{\mathbf{s}}_o; \hat{\mathbf{p}}) f(\mathbf{r}_o, \hat{\mathbf{s}}_o), \tag{3}$$

$$f(\mathbf{r}_o, \hat{\mathbf{s}}_o) = [\mathcal{H}^\dagger g](\mathbf{r}_o, \hat{\mathbf{s}}_o) = \int_{\mathbb{S}^1} d\hat{\mathbf{p}} \int_{\mathbb{R}^2} d\mathbf{r}_d\, h(\mathbf{r}_d - \mathbf{r}_o, \hat{\mathbf{s}}_o; \hat{\mathbf{p}}) g(\mathbf{r}_d, \hat{\mathbf{p}}), \tag{4}$$

where $f(\mathbf{r}_o, \hat{\mathbf{s}}_o)$ is the object, $g(\mathbf{r}_d, \hat{\mathbf{p}})$ is the data, and $h(\mathbf{r}_d - \mathbf{r}_o, \hat{\mathbf{s}}_o; \hat{\mathbf{p}})$ is the kernel of the integral transform. The kernel can be interpreted as a "point spread function" if we visualize the complete data space as a "donut" of images. A delta function at a point in object space will give rise to the kernel evaluated at that point in data space.

We can write the forward and adjoint operators in the frequency domain as

$$G_n(\boldsymbol{\nu}) = \sum_{l=0}^{\infty} \sum_{m=-l}^{l} H_{l,n}^m(\boldsymbol{\nu}) F_l^m(\boldsymbol{\nu}), \tag{5}$$

$$F_l^m(\boldsymbol{\nu}) = \sum_{n=-\infty}^{\infty} H_{l,n}^m(\boldsymbol{\nu}) G_n(\boldsymbol{\nu}), \tag{6}$$

where

$$G_n(\boldsymbol{\nu}) = \int_{\mathbb{S}^1} d\hat{\mathbf{p}}\, z_n(\hat{\mathbf{p}}) \int_{\mathbb{R}^2} d\mathbf{r}_d\, \mathrm{e}^{i2\pi \mathbf{r}_d \cdot \boldsymbol{\nu}} g(\mathbf{r}_d, \hat{\mathbf{p}}), \tag{7}$$

$$H_{l,n}^m(\boldsymbol{\nu}) = \int_{\mathbb{S}^1} d\hat{\mathbf{p}}\, z_n(\hat{\mathbf{p}}) \int_{\mathbb{S}^2} d\hat{\mathbf{s}}_o\, y_l^m(\hat{\mathbf{s}}_o) \int_{\mathbb{R}^2} d\mathbf{r}_o\, \mathrm{e}^{i2\pi \mathbf{r}_o \cdot \boldsymbol{\nu}} h(\mathbf{r}_o, \hat{\mathbf{s}}_o; \hat{\mathbf{p}}), \tag{8}$$

$$F_l^m(\boldsymbol{\nu}) = \int_{\mathbb{S}^2} d\hat{\mathbf{s}}_o\, y_l^m(\hat{\mathbf{s}}_o) \int_{\mathbb{R}^2} d\mathbf{r}_o\, \mathrm{e}^{i2\pi \mathbf{r}_o \cdot \boldsymbol{\nu}} f(\mathbf{r}_o, \hat{\mathbf{s}}_o). \tag{9}$$

To find the singular value decomposition of the forward operator, we need to solve

$$\mathcal{H}\mathcal{H}^\dagger v_{\boldsymbol{\rho},j}(\mathbf{r}_d, \hat{\mathbf{p}}) = \mu_{\boldsymbol{\rho},j} v_{\boldsymbol{\rho},j}(\mathbf{r}_d, \hat{\mathbf{p}}). \tag{10}$$

It is much easier to solve the equivalent problem in the frequency domain

$$\mathsf{K}(\boldsymbol{\rho})\mathsf{V}_j(\boldsymbol{\rho}) = \mu_{\boldsymbol{\rho},j} \mathsf{V}_j(\boldsymbol{\rho}). \tag{11}$$

where the entries of $\mathsf{K}(\boldsymbol{\rho})$ are given by

$$K_{nn'}(\boldsymbol{\rho}) = \sum_{l=0}^{\infty} \sum_{m=-l}^{l} H_{l,n}^m(\boldsymbol{\rho}) H_{l,n'}^m(\boldsymbol{\rho}), \tag{12}$$

and the entries of $\mathsf{V}_j(\boldsymbol{\rho})$ are related to the complete data space singular functions by

$$v_{\boldsymbol{\rho},j}(\mathbf{r}_d, \hat{\mathbf{p}}) = \mathrm{e}^{i2\pi \boldsymbol{\rho} \cdot \mathbf{r}_d} \sum_{n=-\infty}^{\infty} [V_n(\boldsymbol{\rho})]_j z_n(\hat{\mathbf{p}}). \tag{13}$$

Once we've found the data space singular functions, we can find the object space singular functions using

$$[U_l^m(\boldsymbol{\rho})]_j = \sum_{n=-\infty}^{\infty} H_{l,n}^m(\boldsymbol{\rho}) [V_n(\boldsymbol{\rho})]_j, \tag{14}$$

$$u_{\boldsymbol{\rho},j}(\mathbf{r}_o, \hat{\mathbf{s}}_o) = \mathrm{e}^{i2\pi \boldsymbol{\rho} \cdot \mathbf{r}_o} \sum_{l=0}^{\infty} \sum_{m=-l}^{l} [U_l^m(\boldsymbol{\rho})]_j y_l^m(\hat{\mathbf{s}}_o). \tag{15}$$

3 Polarized illumination

3.1 Kernel

In previous notes we showed that the excitation point response function for polarized epi-illumination is given by

$$h_{\mathrm{exc}}^{\hat{\mathbf{z}}}(\hat{\mathbf{s}}_o; \hat{\mathbf{p}}) = y_0^0(\hat{\mathbf{s}}_o) - \frac{1}{\sqrt{5}} \tilde{A} y_2^0(\hat{\mathbf{s}}_o) + \sqrt{\frac{3}{5}} \tilde{B} \left\{ [(\hat{\mathbf{p}} \cdot \hat{\mathbf{x}})^2 - (\hat{\mathbf{p}} \cdot \hat{\mathbf{y}})^2] y_2^2(\hat{\mathbf{s}}_o) - 2(\hat{\mathbf{p}} \cdot \hat{\mathbf{x}})(\hat{\mathbf{p}} \cdot \hat{\mathbf{y}}) y_2^{-2}(\hat{\mathbf{s}}_o) \right\}, \tag{16}$$

where

$$\tilde{A} \equiv \cos^2(\alpha/2)\cos(\alpha), \tag{17a}$$

$$\tilde{B} \equiv \frac{1}{12}(\cos^2\alpha + 4\cos\alpha + 7), \tag{17b}$$

and $\alpha \equiv \arcsin(\mathrm{NA}/n_o)$. It is more convenient to write the point response function in terms of the circular harmonics

$$h_{\mathrm{exc}}^{\hat{\mathbf{z}}}(\hat{\mathbf{s}}_o;\hat{\mathbf{p}}) = y_0^0(\hat{\mathbf{s}}_o) - \frac{1}{\sqrt{5}}\tilde{A}y_2^0(\hat{\mathbf{s}}_o) + \sqrt{\frac{3}{5}}\tilde{B}\left\{y_2^2(\hat{\mathbf{s}}_o)z_2(\hat{\mathbf{p}}) - y_2^{-2}(\hat{\mathbf{s}}_o)z_{-2}(\hat{\mathbf{p}})\right\}. \tag{18}$$

We derived this excitation kernel using the model from Chandler et al. [1]—a model modified from Fourkas [2]. Both papers claim that their equations model aplanatic (shift-invariant) objectives, but this is not strictly true. Fourkas and Chandler ignore the $1/\sqrt{\cos\theta}$ apodization factor for aplanatic objectives and unknowingly model a non-aplanatic objective that satisfies the Herschel condition instead of Abbe's sine condition. The difference between these models is small but non-zero under the paraxial approximation.

In the most recent string of note sets I have been modeling a true aplanatic objective under the paraxial approximation. The correct paraxial excitation model for an aplanatic objective is

$$h_{\mathrm{exc}}^{(\mathrm{ap}),\hat{\mathbf{z}}}(\hat{\mathbf{s}}_o;\hat{\mathbf{p}}) = y_0^0(\hat{\mathbf{s}}_o) - \frac{1}{\sqrt{5}}\left[1 - 2\left(\frac{\mathrm{NA}}{n_o}\right)^2\right]y_2^0(\hat{\mathbf{s}}_o) + \sqrt{\frac{3}{5}}\left\{y_2^2(\hat{\mathbf{s}}_o)z_2(\hat{\mathbf{p}}) - y_2^{-2}(\hat{\mathbf{s}}_o)z_{-2}(\hat{\mathbf{p}})\right\}. \tag{19}$$

We will drop the (ap) superscript unless there is possibility for confusion. Eq. 19 shows that for an aplanatic objective under the paraxial approximation, the y_2^0 term is excited less relative to the y_0^0 term as the NA increases (recall that the kernel is normalized). We also see that the y_2^2 and y_2^{-2} terms do not depend on the NA, but they do depend on the polarizer orientation.

Relevant discussion of Abbe's sine condition, the Herschel condition, apodization functions, and the paraxial approximation can be found in Barrett 9.6.7 [3], Mansuripur 1.0 [4], and especially Gu 6.3 [5]. Although we (and Fourkas) incorrectly stated that we were modeling an aplanatic objective in [1], we brought attention to our lack of apodization in the discussion section. All of our major conclusions would still hold if we used the correct apodization (and our numerical results hold for Herschel objectives although these are rarely used in microscopy).

We also showed that the kernel for unpolarized epi-detection is given by

$$h_{\mathrm{det}}(\mathbf{r}_o,\hat{\mathbf{s}}_o) = [a^2(r_o) + 2b^2(r_o)]y_0^0(\hat{\mathbf{s}}_o) + \frac{1}{\sqrt{5}}\left[-a^2(r_o) + 4b^2(r_o)\right]y_2^0(\hat{\mathbf{s}}_o), \tag{20}$$

where

$$a(r_o) = \frac{J_1(2\pi\nu_o r_o)}{\pi\nu_o r_o}, \qquad b(r_o) = \frac{\mathrm{NA}}{n_o}\left[\frac{J_2(2\pi\nu_o r_o)}{\pi\nu_o r_o}\right], \tag{21}$$

and

$$\nu_o \equiv \frac{\mathrm{NA}}{\lambda}, \qquad \mathrm{NA} = n_o\sin\alpha. \tag{22}$$

The excitation and detection processes are incoherent, so to find the complete kernel we multiply the excitation and detection kernels

$$h(\mathbf{r}_o,\hat{\mathbf{s}}_o;\hat{\mathbf{p}}) = h_{\mathrm{exc}}^{\hat{\mathbf{z}}}(\hat{\mathbf{s}}_o;\hat{\mathbf{p}})h_{\mathrm{det}}(\mathbf{r}_o,\hat{\mathbf{s}}_o) = \sum_{l=0}^{\infty}\sum_{m=-l}^{l}\sum_{n=-\infty}^{\infty} h_{l,n}^m(\mathbf{r}_o)y_l^m(\hat{\mathbf{s}}_o)z_n(\hat{\mathbf{p}}). \tag{23}$$

In previous notes we were able to calculate these products in terms of the circular and spherical harmonics by hand, but this is time consuming and error prone. To simplify the multiplication we precompute the triple integrals of the circular and spherical harmonics and compute the product using a tensor product—see Appendix A for details.

We can write a closed form expression for the kernel, but the expression is long and not particularly useful. Instead, we plot each term of the kernel in Fig. 1.

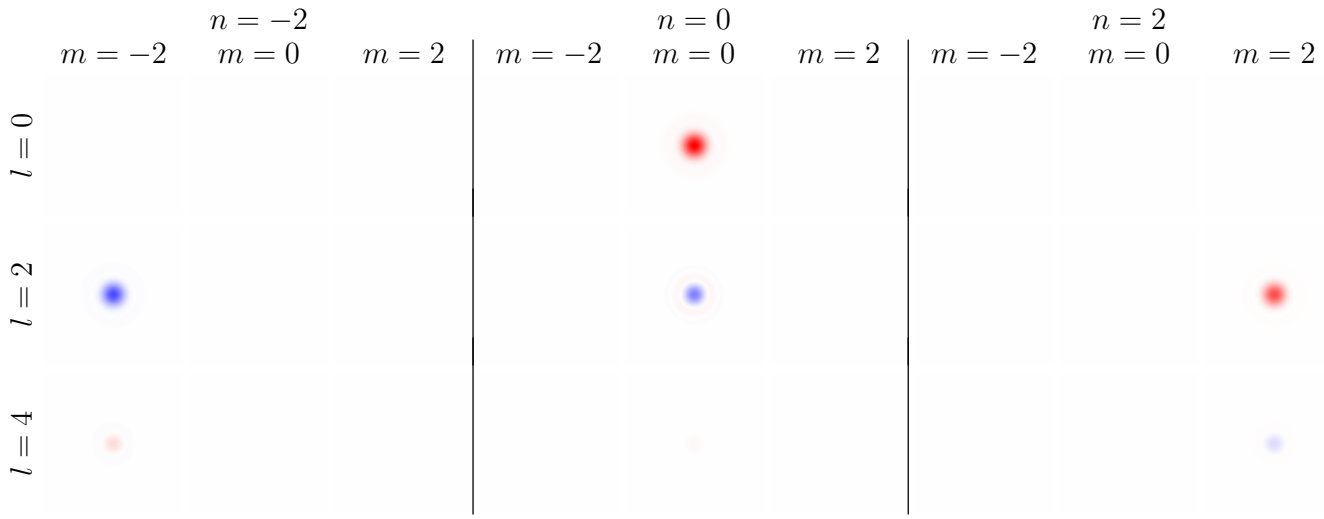

Figure 1: Five-dimensional kernel $h^m_{l,n}(\mathbf{r}_o)$ for a single-view polarized illumination microscope with 0.8 NA epi-illumination and epi-detection. **Rows:** l indexes the object-space spherical harmonic band. **Columns:** m indexes the object-space spherical harmonic degree, and n indexes the data-space circular harmonic band. **Entries:** Each column and row contains a continuous two-dimensional plot indexed by the vector $\mathbf{r}_o$ ranging from $-2\lambda/\text{NA}$ to $+2\lambda/\text{NA}$ (although $\mathbf{r}_o$ is rotationally symmetric so one dimension would suffice). All values are normalized between -1 (blue) and $+1$ (red) with 0 colored white.

Each of the (l, m, n) terms of the kernel shown in Fig. 1 can be interpreted as the shape of the $z_n(\hat{\mathbf{p}})$ component of the intensity pattern detected when the object consists of $y^m_l(\hat{\mathbf{s}}_o)$ distributed dipoles. For example, the $l = 0$, $m = 0$, $n = 0$ term shows the intensity pattern for the $z_0(\hat{\mathbf{p}})$ (constant) component detected when the object consists of $y^0_0(\hat{\mathbf{s}}_o)$ (uniformly distributed) dipoles. Notice that the $l = 0$, $m = 0$, $n = \pm 2$ terms are zero which means that the intensity pattern from a uniform distribution of fluorophores is independent of the polarizer orientation.

Interestingly, every (l, m) term in the kernel has a single n term that is non-zero. This means that each spherical harmonic component in object space gives rise to a single circular harmonic component in data space. This property is specific to polarized illumination microscopes.

Finally, notice that the polarizer dimension is limited to $n = \{-2, 0, 2\}$. The three terms mean that three polarizer orientations are sufficient to completely sample that dimension. We have suspected that three measurements are sufficient because the polarization dependence of an intensity signal can be specified with three numbers—an offset, an amplitude, and a phase. The three circular harmonic components of the signal capture the same information as the offset, amplitude, and phase; and they are orthogonal functions so they allow us to use frequency domain techniques.

3.2 Transfer function

We can calculate the transfer function using Eq. 8 and the kernel, but this will lead to a very long expression. Instead, we calculate the illumination transfer function and the detection transfer function then use the multiplication rules in Appendix A to find the complete transfer function.

The illumination transfer function is

$$H^m_{\mathrm{exc},l,n} = \delta_{l,0}\delta_{m,0}\delta_{n,0} - \frac{1}{\sqrt{5}}\left[1 - 2\left(\frac{\mathrm{NA}}{n_o}\right)^2\right]\delta_{l,2}\delta_{m,0}\delta_{n,0} + \sqrt{\frac{3}{5}}\left\{\delta_{l,2}\delta_{m,2}\delta_{n,2} - \delta_{l,-2}\delta_{m,-2}\delta_{n,-2}\right\}, \tag{24}$$

and the detection transfer function is

$$H^m_{\mathrm{det},l,n}(\nu) = [A(\nu) + 2B(\nu)]\delta_{l,0}\delta_{m,0}\delta_{n,0} + \frac{1}{\sqrt{5}}\left[-A(\nu) + 4B(\nu)\right]\delta_{l,2}\delta_{m,0}\delta_{n,0}, \tag{25}$$

where

$$A(\nu) = \frac{2}{\pi}\left[\arccos\left(\frac{\nu}{2\nu_o}\right) - \frac{\nu}{2\nu_o}\sqrt{1 - \left(\frac{\nu}{2\nu_o}\right)^2}\right]\Pi\left(\frac{\nu}{2\nu_o}\right), \tag{26}$$

$$B(\nu) = \frac{1}{\pi}\left(\frac{\mathrm{NA}}{n_o}\right)^2\left[\arccos\left(\frac{\nu}{2\nu_o}\right) - \left[3 - 2\left(\frac{\nu}{2\nu_o}\right)^2\right]\frac{\nu}{2\nu_o}\sqrt{1 - \left(\frac{\nu}{2\nu_o}\right)^2}\right]\Pi\left(\frac{\nu}{2\nu_o}\right). \tag{27}$$

The complete transfer function is given by

$$H^m_{l,n}(\nu) = H^m_{\mathrm{exc},l,n} * H^m_{\mathrm{det},l,n}(\nu), \tag{28}$$

where $*$ denotes a generalized convolution over all five indices. In Appendix A we show how to evaluate the convolution over the discrete indices. The excitation pattern is spatially uniform, so the spatial convolution is trivial. We plot the complete transfer function in Fig. 2.

3.3 Singular value decomposition

Plugging the transfer function into the frequency-domain eigenvalue problem (Eq. 11) yields a denumerably infinite eigenvalue problem with only 3×3 non-zero entries in the matrix (we suppress the index $\boldsymbol{\rho}$ and understand that we need to solve this eigenvalue problem at each value of $\boldsymbol{\rho}$)

$$\mathsf{K}\mathsf{V}_j = \mu_j\mathsf{V}_j, \tag{29}$$

$$\begin{bmatrix} \sum_{l,m} H^m_{l,-2}H^m_{l,-2} & \sum_{l,m} H^m_{l,-2}H^m_{l,0} & \sum_{l,m} H^m_{l,-2}H^m_{l,2} \\ \sum_{l,m} H^m_{l,0}H^m_{l,-2} & \sum_{l,m} H^m_{l,0}H^m_{l,0} & \sum_{l,m} H^m_{l,0}H^m_{l,2} \\ \sum_{l,m} H^m_{l,2}H^m_{l,-2} & \sum_{l,m} H^m_{l,2}H^m_{l,0} & \sum_{l,m} H^m_{l,2}H^m_{l,2} \end{bmatrix}\mathsf{V}_j = \mu_j\mathsf{V}_j, \tag{30}$$

$$\begin{bmatrix} \{H^{-2}_{2,-2}\}^2 + \{H^{-2}_{4,-2}\}^2 & 0 & 0 \\ 0 & \{H^0_{0,0}\}^2 + \{H^0_{2,0}\}^2 + \{H^0_{4,0}\}^2 & 0 \\ 0 & 0 & \{H^2_{2,2}\}^2 + \{H^2_{4,2}\}^2 \end{bmatrix}\mathsf{V}_j = \mu_j\mathsf{V}_j. \tag{31}$$

A diagonal matrix has its eigenvalues along the diagonal and its eigenvectors as unit vectors so

$$\mu_{\boldsymbol{\rho},0} = \{H^0_{0,0}(\rho)\}^2 + \{H^0_{2,0}(\rho)\}^2 + \{H^0_{4,0}(\rho)\}^2, \tag{32}$$

$$\mu_{\boldsymbol{\rho},1} = \mu_{\boldsymbol{\rho},2} = \{H^2_{2,2}(\rho)\}^2 + \{H^2_{4,2}(\rho)\}^2, \tag{33}$$

and

$$\mathsf{V}_0 = \begin{bmatrix}0\\1\\0\end{bmatrix}, \qquad \mathsf{V}_1 = \begin{bmatrix}1\\0\\0\end{bmatrix}, \qquad \mathsf{V}_2 = \begin{bmatrix}0\\0\\1\end{bmatrix}. \tag{34}$$

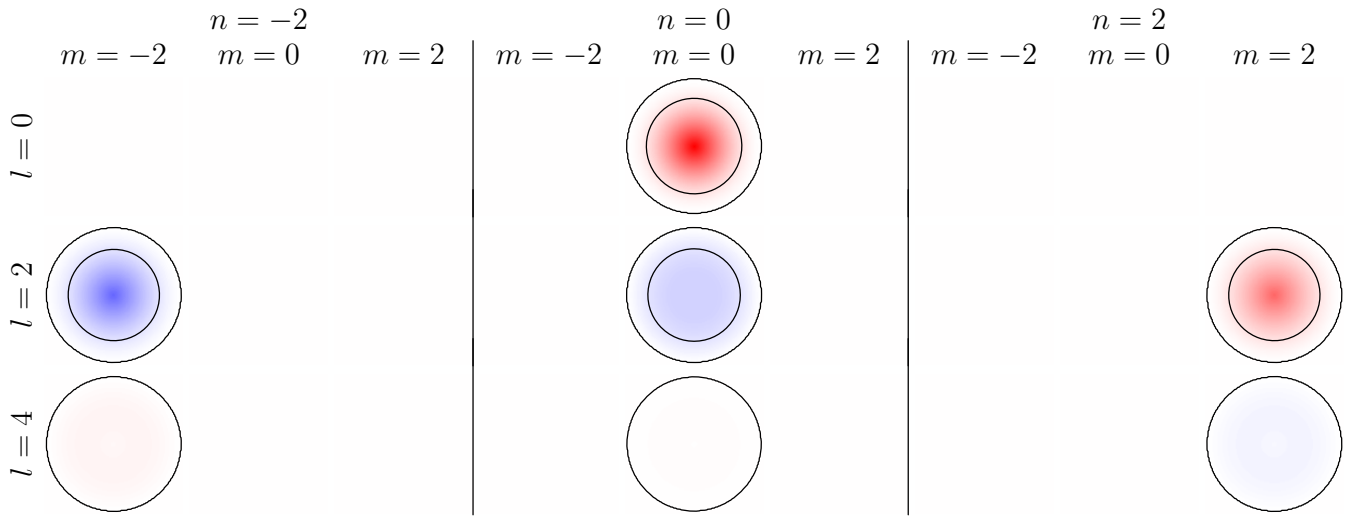

Figure 2: Five-dimensional transfer function $H^m_{l,n}(\boldsymbol{\nu})$ for a single-view polarized illumination microscope with 0.8 NA epi-illumination and epi-detection. **Rows:** l indexes the object-space spherical harmonic band. **Columns:** m indexes the object-space spherical harmonic degree, and n indexes the data-space circular harmonic band. **Entries:** Each column and row contains a continuous two-dimension plot indexed by the vector $\boldsymbol{\nu}$ ranging from $-2\text{NA}/\lambda$ to $+2\text{NA}/\lambda$. All values are normalized between -1 (blue) and $+1$ (red) with 0 colored white. Black lines are contours at 0 and ± 0.1.

Notice that we have two degenerate eigenvalues, but we have found trivial orthonormal eigenvectors—in general we will need to apply the Gram-Schmidt procedure.

We can use Eq. 13 to recover the complete singular functions in data space as

$$v_{\boldsymbol{\rho},0}(\mathbf{r}_d, \hat{\mathbf{p}}) = \mathrm{e}^{i2\pi\boldsymbol{\rho}\cdot\mathbf{r}_d} z_0(\hat{\mathbf{p}}), \tag{35}$$
$$v_{\boldsymbol{\rho},1}(\mathbf{r}_d, \hat{\mathbf{p}}) = \mathrm{e}^{i2\pi\boldsymbol{\rho}\cdot\mathbf{r}_d} z_{-2}(\hat{\mathbf{p}}), \tag{36}$$
$$v_{\boldsymbol{\rho},2}(\mathbf{r}_d, \hat{\mathbf{p}}) = \mathrm{e}^{i2\pi\boldsymbol{\rho}\cdot\mathbf{r}_d} z_2(\hat{\mathbf{p}}). \tag{37}$$

For the final step we use Eq. 14 to find the spectra of the singular functions in object space

$$[U^m_l(\rho)]_0 = H^m_{l,0}(\rho) = H^0_{0,0}(\rho)\delta_{l0}\delta_{m0} + H^0_{2,0}(\rho)\delta_{l2}\delta_{m0} + H^0_{4,0}(\rho)\delta_{l4}\delta_{m0}, \tag{38}$$
$$[U^m_l(\rho)]_1 = H^m_{l,-2}(\rho) = H^{-2}_{2,-2}(\rho)\delta_{l2}\delta_{m-2} + H^{-2}_{4,-2}(\rho)\delta_{l4}\delta_{m-2}, \tag{39}$$
$$[U^m_l(\rho)]_2 = H^m_{l,2}(\rho) = H^m_{l,2}(\rho) = H^2_{2,2}(\rho)\delta_{l2}\delta m2 + H^2_{4,2}(\rho)\delta_{l4}\delta_{m2}. \tag{40}$$

Therefore, the complete singular functions in object space are

$$u_{\boldsymbol{\rho},0}(\mathbf{r}_o, \hat{\mathbf{s}}_o) = \mathrm{e}^{i2\pi\boldsymbol{\rho}\cdot\mathbf{r}_o}[H^0_{0,0}(\rho)y^0_0(\hat{\mathbf{s}}_o) + H^0_{2,0}(\rho)y^0_2(\hat{\mathbf{s}}_o) + H^0_{4,0}(\rho)y^0_4(\hat{\mathbf{s}}_o)], \tag{41}$$
$$u_{\boldsymbol{\rho},1}(\mathbf{r}_o, \hat{\mathbf{s}}_o) = \mathrm{e}^{i2\pi\boldsymbol{\rho}\cdot\mathbf{r}_o}[H^{-2}_{2,-2}(\rho)y^{-2}_2(\hat{\mathbf{s}}_o) + H^{-2}_{4,-2}(\rho)y^{-2}_4(\hat{\mathbf{s}}_o)], \tag{42}$$
$$u_{\boldsymbol{\rho},2}(\mathbf{r}_o, \hat{\mathbf{s}}_o) = \mathrm{e}^{i2\pi\boldsymbol{\rho}\cdot\mathbf{r}_o}[H^2_{2,2}(\rho)y^2_2(\hat{\mathbf{s}}_o) + H^2_{4,2}(\rho)y^2_4(\hat{\mathbf{s}}_o)]. \tag{43}$$

Finally, the singular values are the square root of the eigenvalues

$$\sigma_{\boldsymbol{\rho},j} = \sqrt{\mu_{\boldsymbol{\rho},j}}. \tag{44}$$

We have found the complete singular system for a single view microscope with polarized illumination. In Fig. 3 we show all three branches of the singular spectrum along with the angular part of the object space singular functions $u_{\boldsymbol{\rho},j}(0, \hat{\mathbf{s}}_o)$.

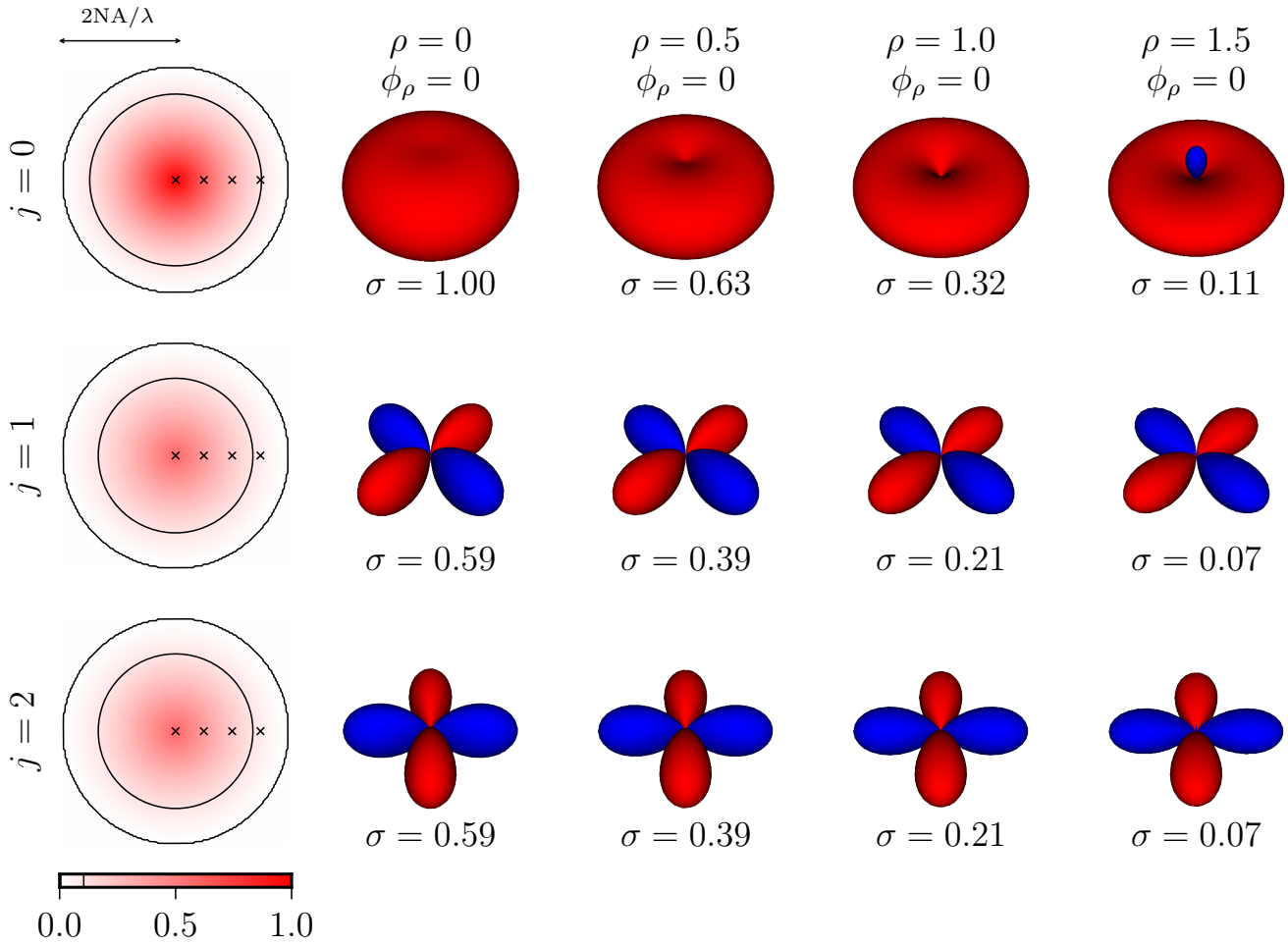

Figure 3: Singular system for a single-view polarized illumination microscope with 0.8 NA epi-illumination and epi-detection. **Rows:** Discrete branches of the singular value system indexed by j. **Column 1:** Continuous singular value spectra for each branch j indexed by spatial frequency $\boldsymbol{\rho}$. The singular value spectra are normalized with contour lines at 0 and 0.1. **Columns 2-5:** Angular part of the object-space singular vector at spatial frequencies marked with 'x's in the first column. The camera is facing the origin along the [1,1,1] axis with the optical axis of the microscope pointing up along the page. A red surface indicates positive values, a blue surface indicates negative values, and the distance from the origin indicates the magnitude.

All three branches of the singular system have object-space singular functions that depend on the spatial frequency (the plots in each column and row of Fig. 3 are different). This dependence is largest in the $j = 0$ branch where at low spatial frequencies the singular functions are nearly spherical, while at high spatial frequencies the singular functions are negative along the optical axis. The fact that the singular functions of the $j = 0$ branch are non-spherical and have a spatial-frequency dependence is the most important result of this section—it means that a single view microscope can distinguish distributions of fluorophores that have different out-of-transverse-plane components. The $j = 1$ and $j = 2$ object-space singular functions still depend on the spatial frequency—the high-frequency singular functions are "flatter" in the transverse plane than the low-frequency singular functions—but this dependence is relatively small.

We can use the singular value spectrum to find the degeneracies and symmetries of the microscope. The first major set of degeneracies is related to the fact that $\sigma_{\boldsymbol{\rho},1} = \sigma_{\boldsymbol{\rho},2}$. The corresponding singular functions in object space are related by changing the spherical harmonic index m to $-m$. This transformation is a rotation about the optical axis, so this degeneracy corresponds to the rotational symmetry of the microscope. The

second set of degeneracies is related to the fact that the singular values depend only on ρ, not the vector $\boldsymbol{\rho}$. The corresponding singular functions in object space are spatial harmonics at the same spatial frequency in different directions. Once again, this degeneracy corresponds to the rotational symmetry of the microscope.

Recall the mental image of data space being arranged on a donut. If we rotate the object that we are imaging then the data space will undergo two simultaneous rotations—one rotation about an axis through the donut hole (imagine sticking your finger through the donut) and another about the curved axis that runs through the center of the dough (imagine twisting the donut in on itself so that glaze on top would end up on the bottom). These two simultaneous rotations correspond with the two sets of degeneracies we see in the singular value spectrum.

We have only plotted the object space singular functions for spatial frequencies along the x-axis, but these are sufficient to characterize the singular functions for any spatial frequency direction. To see this, notice that the $j = 0$ singular functions are rotationally symmetric about the optical axis and the $j = 1$ and $j = 2$ singular functions are degenerate and they span a rotationally symmetric space of singular functions.

4 Polarized detection

We'll use the same notation as the previous section, so there will be notation overlap.

4.1 Kernel

Earlier we showed that the excitation point response function for unpolarized epi-illumination is given by

$$h_{\text{exc}}^{\hat{\mathbf{z}}}(\hat{\mathbf{s}}_o) = y_0^0(\hat{\mathbf{s}}_o) - \frac{1}{\sqrt{5}}\left[1 - 2\left(\frac{\text{NA}}{n_o}\right)^2\right] y_2^0(\hat{\mathbf{s}}_o). \tag{45}$$

We also showed that the point response function for polarized detection is given by (rewritten in terms of the circular harmonics)

$$h_{\text{det}}(\mathbf{r}_o, \hat{\mathbf{s}}_o; \hat{\mathbf{p}}) = \sum_{l=0}^{\infty} \sum_{m=-l}^{l} \sum_{n=-\infty}^{\infty} h_{\text{det},l,n}^m(\mathbf{r}_o) y_l^m(\hat{\mathbf{s}}_o) z_n(\hat{\mathbf{p}}_d), \tag{46}$$

where

$$h_{\text{det},0,0}^0(\mathbf{r}_o) = a^2(r_o) + 2b^2(r_0), \tag{47}$$

$$h_{\text{det},0,\pm 2}^0(\mathbf{r}_o) = 2\sqrt{\pi} b^2(r_0) z_{\pm 2}(\mathbf{r}_o), \tag{48}$$

$$h_{\text{det},2,0}^0(\mathbf{r}_o) = \frac{1}{\sqrt{5}}\left[-a^2(r_o) + 4b^2(r_0)\right], \tag{49}$$

$$h_{\text{det},2,\pm 2}^0(\mathbf{r}_o) = 4\sqrt{\frac{\pi}{5}} b^2(r_0) z_{\pm 2}(\mathbf{r}_o), \tag{50}$$

$$h_{\text{det},2,2}^2(\mathbf{r}_o) = -h_{\text{det},2,-2}^{-2}(\mathbf{r}_o) = \sqrt{\frac{3}{5}} a^2(r_o). \tag{51}$$

The complete kernel for unpolarized illumination and polarized detection is given by the product of the excitation and detection kernels. We plot the result in Fig. 4.

In the polarized illumination case every (l, m) term in the kernel had a single n term that is non-zero. For polarized detection this is no longer true—for example there are non-zero components for $l = 0$, $m = 0$ in the $n = 0, \pm 2$ terms. This means that each spherical harmonic component in object space gives rise to multiple circular harmonic components in data space.

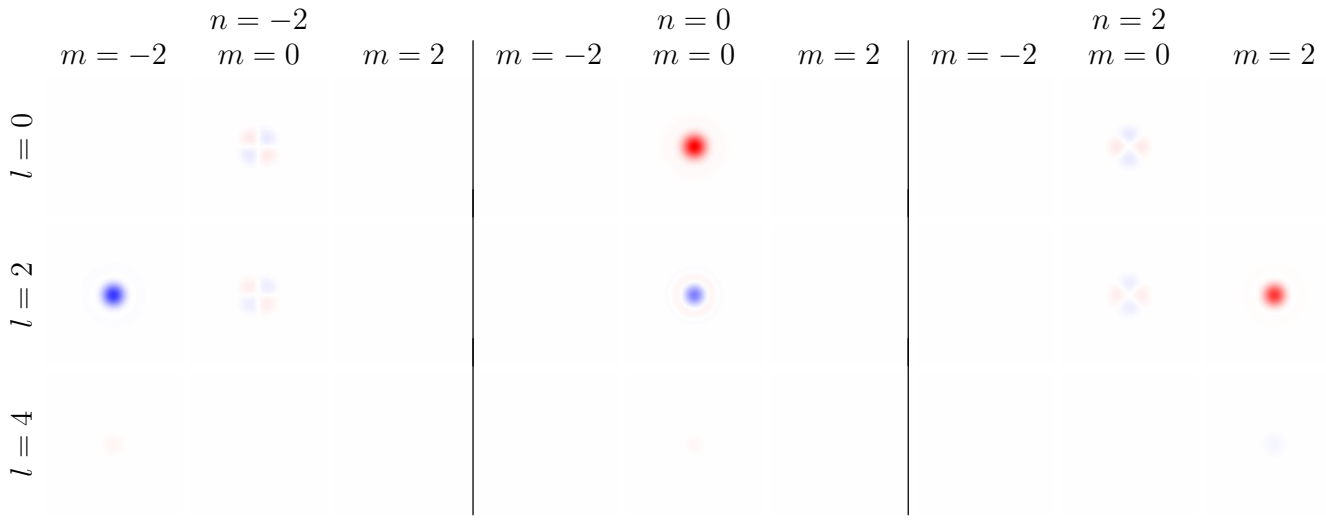

Figure 4: Five-dimensional kernel $h^m_{l,n}(\mathbf{r}_o)$ for a single-view polarized detection microscope with 0.8 NA epi-illumination and epi-detection. **Rows:** l indexes the object-space spherical harmonic band. **Columns:** m indexes the object-space spherical harmonic degree, and n indexes the data-space circular harmonic band. **Entries:** Each column and row contains a continuous two-dimensional plot indexed by the vector $\mathbf{r}_o$ ranging from $-2\lambda/\text{NA}$ to $+2\lambda/\text{NA}$ (although $\mathbf{r}_o$ is rotationally symmetric so one dimension would suffice). All values are normalized between -1 (blue) and $+1$ (red) with 0 colored white.

4.2 Transfer function

The transfer function for unpolarized illumination is

$$H^m_{\text{exc},l,n} = \delta_{l,0}\delta_{m,0}\delta_{n,0} - \frac{1}{\sqrt{5}}\left[1 - 2\left(\frac{\text{NA}}{n_o}\right)^2\right]\delta_{l,2}\delta_{m,0}\delta_{n,0}, \tag{52}$$

and the transfer function for polarized detection is

$$H^m_{\text{det},l,n}(\boldsymbol{\nu}) = \sum_{l=0}^{\infty}\sum_{m=-l}^{l}\sum_{n=-\infty}^{\infty} H^m_{\text{det},l,n}(\boldsymbol{\nu})\delta_{l,l'}\delta_{m,m'}\delta_{n,n'}, \tag{53}$$

where

$$H^0_{\text{det},0,0}(\boldsymbol{\nu}) = A(\nu) + 2B(\nu), \tag{54}$$

$$H^0_{\text{det},0,\pm2}(\boldsymbol{\nu}) = 2\sqrt{\pi}C(\nu)z_{\pm2}(\boldsymbol{\nu}), \tag{55}$$

$$H^0_{\text{det},2,0}(\boldsymbol{\nu}) = \frac{1}{\sqrt{5}}\left[-A(\nu) + 4B(\nu)\right], \tag{56}$$

$$H^0_{\text{det},2,\pm2}(\boldsymbol{\nu}) = 4\sqrt{\frac{\pi}{5}}C(\nu)z_{\pm2}(\boldsymbol{\nu}), \tag{57}$$

$$H^2_{\text{det},2,2}(\boldsymbol{\nu}) = -H^{-2}_{\text{det},2,-2}(\boldsymbol{\nu}) = \sqrt{\frac{3}{5}}A(\nu). \tag{58}$$

and

$$C(\nu) = \frac{1}{\pi}\left(\frac{\text{NA}}{n_o}\right)^2\left[-\frac{4}{3}\frac{\nu}{2\nu_o}\sqrt[3]{1 - \left(\frac{\nu}{2\nu_o}\right)^2}\right]\Pi\left(\frac{\nu}{2\nu_o}\right). \tag{59}$$

Fig. 5 shows the complete transfer function for a polarized detection microscope.

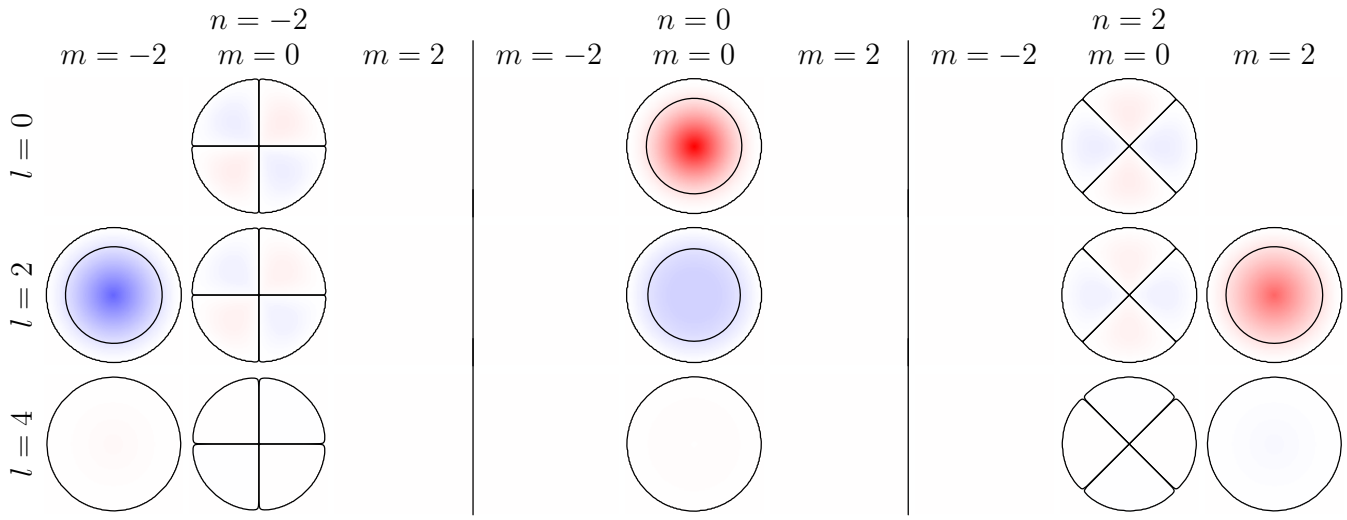

Figure 5: Five-dimensional transfer function $H^m_{l,n}(\boldsymbol{\nu})$ for a single-view polarized detection microscope with 0.8 NA epi-illumination and epi-detection. **Rows:** l indexes the object-space spherical harmonic band. **Columns:** m indexes the object-space spherical harmonic degree, and n indexes the data-space circular harmonic band. **Entries:** Each column and row contains a continuous two-dimension plot indexed by the vector $\boldsymbol{\nu}$ ranging from $-2\text{NA}/\lambda$ to $+2\text{NA}/\lambda$. All values are normalized between -1 (blue) and $+1$ (red) with 0 colored white. Black lines are contours at 0 and ± 0.1.

4.3 Singular value decomposition

We follow the same procedure and plug the transfer function into the frequency-domain eigenvalue problem (Eq. 11) which gives a 3×3 eigenvalue problem

$$\mathsf{K}\mathsf{V}_j = \mu_j \mathsf{V}_j, \tag{60}$$

where the entries of K are given by

$$\mathsf{K}_{00} = \sum_{l,m} H^m_{l,-2} H^m_{l,-2} = \{H^0_{0,-2}\}^2 + \{H^{-2}_{2,-2}\}^2 + \{H^0_{2,-2}\}^2 + \{H^{-2}_{4,-2}\}^2 + \{H^0_{4,-2}\}^2, \tag{61}$$

$$\mathsf{K}_{11} = \sum_{l,m} H^m_{l,0} H^m_{l,0} = \{H^0_{0,0}\}^2 + \{H^0_{2,0}\}^2 + \{H^0_{4,0}\}^2, \tag{62}$$

$$\mathsf{K}_{22} = \sum_{l,m} H^m_{l,2} H^m_{l,2} = \{H^0_{0,2}\}^2 + \{H^2_{2,2}\}^2 + \{H^0_{2,2}\}^2 + \{H^2_{4,2}\}^2 + \{H^0_{4,2}\}^2, \tag{63}$$

$$\mathsf{K}_{01} = \mathsf{K}_{10} = \sum_{l,m} H^m_{l,-2} H^m_{l,0} = H^0_{0,-2} H^0_{0,0} + H^0_{2,-2} H^0_{2,0} + H^0_{4,-2} H^0_{4,0}, \tag{64}$$

$$\mathsf{K}_{02} = \mathsf{K}_{20} = \sum_{l,m} H^m_{l,-2} H^m_{l,2} = H^0_{0,-2} H^0_{0,2} + H^0_{2,-2} H^0_{2,2} + H^0_{4,-2} H^0_{4,2}, \tag{65}$$

$$\mathsf{K}_{12} = \mathsf{K}_{21} = \sum_{l,m} H^m_{l,0} H^m_{l,2} = H^0_{0,0} H^0_{0,2} + H^0_{2,0} H^0_{2,2} + H^0_{4,0} H^0_{4,2}. \tag{66}$$

The eigenvalues and eigenvectors can be computed in a closed form (and I've done this using a symbolic package), but writing the result would fill several pages with notation and provide little insight. Instead we proceed straight to plots of the singular system shown in Fig. 6.

First, notice that the DC term ($\boldsymbol{\rho} = 0$, $j = 0$) of the polarized detection singular system in Fig. 6 is identical to the DC term of the polarized illumination singular system in FIg. 3. This is a result we've seen

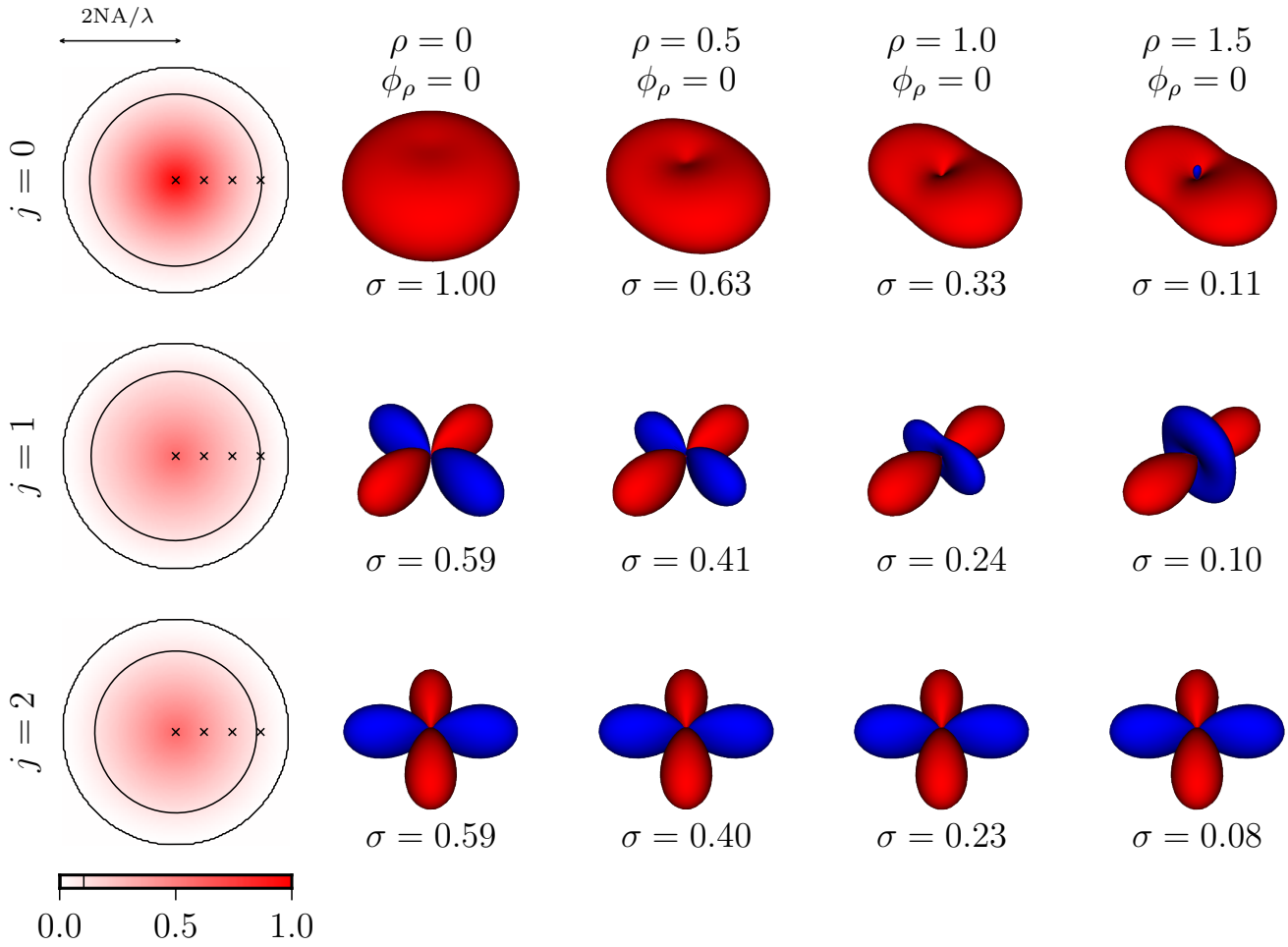

Figure 6: Singular system for a single-view polarized detection microscope with 0.8 NA epi-illumination and epi-detection. **Rows:** Discrete branches of the singular value system indexed by j. **Column 1:** Continuous singular value spectra for each branch j indexed by spatial frequency $\boldsymbol{\rho}$. The singular value spectra are normalized with contour lines at 0 and 0.1. **Columns 2-5:** Angular part of the object-space singular vector at spatial frequencies marked with 'x's in the first column. The camera is facing the origin along the [1,1,1] axis with the optical axis of the microscope pointing up along the page. A red surface indicates positive values, a blue surface indicates negative values, and the distance from the origin indicates the magnitude.

before—if we ignore spatio-angular coupling then polarized illumination and polarized detection microscopes measure identical components of the object.

Second, notice that there are no longer any degeneracies between the three branches of the singular spectrum (except at $\boldsymbol{\rho} = 0$). This means that moving the polarizer to the detection arm breaks a symmetry. Rotating each individual point in object space no longer has a corresponding transformation in data space because the polarizer introduces spatio-angular coupling. Each of the branches of the singular spectrum is still rotationally symmetric, though, so we preserve one of the symmetries—rotating the object about the optical axis will still rotate the data space about the curved axis that runs through the center of donut (the "glaze inversion"!).

Third, notice that the singular values of the polarized detection microscope are larger than the singular values of the polarized illumination microscope at all spatial frequencies except $\boldsymbol{\rho} = 0$ where they are equal. This means that a polarized detection microscope passes orthogonal components of the object more efficiently (the signal is less corruptible by noise) than a polarized illumination microscope. Although the difference is not

extremely large—3-4% at most—this is the most convincing reason that we should prefer polarized detection over polarized illumination.

Finally, consider the singular functions. The singular functions are no longer rotationally symmetric at non-zero spatial frequencies which means that we would see rotated singular functions if we showed the singular functions for spatial frequencies off of the x-axis. We also see that the singular functions contain out-of-plane components at high spatial frequencies (espsecially in the $j = 1$ branch) just like the the polarized illumination case.

References

[1] Talon Chandler, Shalin Mehta, Hari Shroff, Rudolf Oldenbourg, and Patrick J. La Rivière. Single-fluorophore orientation determination with multiview polarized illumination: modeling and microscope design. *Opt. Express*, 25(25):31309–31325, Dec 2017.

[2] John T. Fourkas. Rapid determination of the three-dimensional orientation of single molecules. *Opt. Lett.*, 26(4):211–213, Feb 2001.

[3] H.H. Barrett and K.J. Myers. *Foundations of image science*. Wiley series in pure and applied optics. Wiley-Interscience, 2004.

[4] M. Mansuripur. *Classical Optics and Its Applications*. Classical Optics and Its Applications. Cambridge University Press, 2002.

[5] M. Gu. *Advanced Optical Imaging Theory*. Springer Series in Optical Sciences. Springer, 2000.

[6] Herbert H.H. Homeier and E.Otto Steinborn. Some properties of the coupling coefficients of real spherical harmonics and their relation to gaunt coefficients. *Journal of Molecular Structure: THEOCHEM*, 368:31 – 37, 1996. Proceedings of the Second Electronic Computational Chemistry Conference.

[7] http://docs.sympy.org/latest/modules/physics/wigner.html#sympy.physics.wigner.gaunt.

A Calculating products of circular and spherical harmonics

To calculate the kernels of arbitrary microscope designs we need an efficient way to calculate the products of functions that are linear combinations of circular and spherical harmonics. We start by considering the simplest case of multiplying two linear combinations of circular harmonics given by

$$f(\hat{\mathbf{p}}) = \sum_{n=0}^{\infty} c_n z_n(\hat{\mathbf{p}}), \qquad f'(\hat{\mathbf{p}}) = \sum_{n'=0}^{\infty} c'_{n'} z_{n'}(\hat{\mathbf{p}}). \tag{67}$$

The product of these two functions is given by

$$f''(\hat{\mathbf{p}}) = f(\hat{\mathbf{p}}) f'(\hat{\mathbf{p}}) = \sum_{n=0}^{\infty} \sum_{n'=0}^{\infty} c_n c'_{n'} z_n(\hat{\mathbf{p}}) z_{n'}(\hat{\mathbf{p}}) = \sum_{n''=0}^{\infty} c''_{n''} z_{n''}(\hat{\mathbf{p}}), \tag{68}$$

and we would like to find a relationship between the input coefficients (c_n $c'_{n'}$) and the output coefficients $c''_{n''}$. To find this relationship we can write the product the circular harmonics as a linear combination of circular harmonics

$$z_n(\hat{\mathbf{p}}) z_{n'}(\hat{\mathbf{p}}) = \sum_{j''=0}^{\infty} P_{n,n',n''} z_{j''}(\hat{\mathbf{p}}) \tag{69}$$

where $P_{n,n'}^{n''}$ are the triple integrals of the circular harmonics

$$P_{n,n',n''} = \int_{\mathbb{S}^1} d\hat{\mathbf{p}}\, z_n(\hat{\mathbf{p}}) z_{n'}(\hat{\mathbf{p}}) z_{n''}(\hat{\mathbf{p}}). \tag{70}$$

Plugging Eq. 69 into Eq. 68 gives

$$\sum_{n=0}^{\infty}\sum_{n'=0}^{\infty} c_n c'_{n'} \left[\sum_{j''=0}^{\infty} P_{n,n'}^{n''} z_{j''}(\hat{\mathbf{p}})\right] = \sum_{n''=0}^{\infty} c''_{n''} z_{n''}(\hat{\mathbf{p}}). \tag{71}$$

Therefore, the coefficients are related by

$$c''_{n''} = \sum_{n=0}^{\infty}\sum_{n'=0}^{\infty} P_{n,n',n''} c_n c'_{n'}. \tag{72}$$

Rewriting this equation in Einstein notation (summation over matching indices is implied, upper indices are "column" indices, lower indices are "row" indices) gives

$$c''^{n''} = P_{n,n'}^{n''} c^n c'^{n'}. \tag{73}$$

We can precompute the triple integrals $P_{n,n',n''}$ using a symbolic package like Sympy.

The discussion above applies to spherical harmonics as well—we only need to replace the triple integral of the circular harmonics $P_{n,n',n''}$ with the triple integral of the spherical harmonics

$$G_{j,j',j''} = \int_{\mathbb{S}^2} d\hat{\mathbf{s}}\, y_j(\hat{\mathbf{s}}) y_{j'}(\hat{\mathbf{s}}) y_{j''}(\hat{\mathbf{s}}). \tag{74}$$

where each of the j indices are a single index over the spherical harmonics. We could compute the triple integrals symbolically, but these integrals can take several minutes. Instead, we can write the integral in terms of the Gaunt coefficients [6] which are products of the Clebsch-Gordan coefficients or Wigner 3-j symbols. The Gaunt coefficients have a closed form expression in terms of j, j', and j'' (usually expressed in terms of l, l', l'', m, m', m'') that is implemented in the Sympy library [7].

To calculate the kernel for general polarized light microscopes we will need to multiply functions in the following form

$$f(\hat{\mathbf{p}}, \hat{\mathbf{s}}) = \sum_{n=0}^{\infty}\sum_{j=0}^{\infty} c_{n,j} z_n(\hat{\mathbf{p}}) y_j(\hat{\mathbf{s}}), \qquad f'(\hat{\mathbf{p}}, \hat{\mathbf{s}}) = \sum_{n'=0}^{\infty}\sum_{j'=0}^{\infty} c'_{n',j'} z_n(\hat{\mathbf{p}}) y_j(\hat{\mathbf{s}}). \tag{75}$$

The product will be in the form

$$f(\hat{\mathbf{p}}, \hat{\mathbf{s}}) f'(\hat{\mathbf{p}}, \hat{\mathbf{s}}) = \sum_{n=0}^{\infty}\sum_{j=0}^{\infty} c''_{n'',j''} z_{n''}(\hat{\mathbf{p}}) y_{j''}(\hat{\mathbf{s}}), \tag{76}$$

where

$$c''^{n'',j''} = P_{n,n'}^{n''} G_{j,j'}^{j''} c^{n,j} c'^{n',j'}. \tag{77}$$

Equation 77 is the main result of this section. It shows that we can precalculate the triple integrals of the circular and spherical harmonics and use the results to efficiently find the coefficients of the product of two arbitrary kernels. We can think of Eq. 77 as a bilinear map that acts within the vector space of harmonic function coefficients. The bilinear map takes two elements of the vector space and maps them to another element of the vector space by a rank-6 tensor product. A lower dimensional example of a bilinear map is the cross product which takes two vectors in three-dimensional Euclidean space and maps them to another vector by a rank-3 tensor product.